NIH Public Access
Author Manuscript
Bone. Author manuscript; available in PMC 2009 October 1.

Published in final edited form as:
Bone. 2008 October ; 43(4): 775–780. doi:10.1016/j.bone.2008.05.023.

Identification of material parameters based on Mohr-Coulomb failure criterion for bisphosphonate treated canine vertebral cancellous bone

Xiang Wang[a,b], **Matthew R. Allen**[c], **David B. Burr**[c,d,e], **Enrique J. Lavernia**[f], **Boris Jeremić**[g], and **David P. Fyhrie**[a]

a*Lawrence J. Ellison Musculoskeletal Research Center, University of California Davis Medical Center, Sacramento, CA, USA*

b*Orthopaedic Biomechanics Laboratory, University of California, Berkeley, CA, USA*

c*Department of Anatomy and Cell Biology, Indiana University School of Medicine, Indianapolis, IN, USA*

d*Department of Orthopaedic Surgery, Indiana University School of Medicine, Indianapolis, IN, USA*

e*Biomedical Engineering Program, Indiana University-Purdue University Indianapolis, Indianapolis, IN, USA*

f*Chemical Engineering and Material Science Department, University of California, Davis, CA, USA*

g*Department of Civil and Environmental Engineering, University of California, Davis, CA, USA*

Abstract

Nanoindentation has been widely used to study bone tissue mechanical properties. The common method and equations for analyzing nanoindentation, developed by Oliver and Pharr, are based on the assumption that the material is linearly elastic. In the present study, we adjusted the constraint of linearly elastic behavior and use nonlinear finite element analysis to determine the change in cancellous bone material properties caused by bisphosphonate treatment, based on an isotropic form of the Mohr-Coulomb failure model. Thirty-three canine lumbar vertebrae were used in this study. The dogs were treated daily for 1 year with oral doses of alendronate, risedronate, or saline vehicle at doses consistent, on a mg/kg basis, to those used clinically for the treatment of post-menopausal osteoporosis. Two sets of elastic modulus and hardness values were calculated for each specimen using the Continuous Stiffness Measurement (CSM) method (E_{CSM} and H_{CSM}) from the loading segment and the Oliver-Pharr method ($E_{O\text{-}P}$ and $H_{O\text{-}P}$) from the unloading segment, respectively. Young's modulus (E_{FE}), cohesion (c), and friction angle (ϕ) were identified using a finite element model for each nanoindentation. The bone material properties were compared among groups and between methods for property identification. Bisphosphonate treatment had a significant effect on several of the material parameters. In particular, Oliver-Pharr hardness was larger for both the risedronate- and alendronate-treated groups compared to vehicle and the Mohr-Coulomb cohesion was larger for the risedronate-treated compared to vehicle. This result suggests that bisphosphonate treatment increases the hardness and shear strength of bone tissue. Shear strength was linearly predicted by modulus and hardness measured by the Oliver-Pharr method (r^2=0.99). These results

Please address all correspondence to: Xiang Wang, Ph.D., Email: x10wang@gmail.com, Phone: (916) 202-9749, Orthopaedic Biomechanics Laboratory, 2166 Etcheverry Hall, University of California, Berkeley, CA 94720-1742.

Publisher's Disclaimer: This is a PDF file of an unedited manuscript that has been accepted for publication. As a service to our customers we are providing this early version of the manuscript. The manuscript will undergo copyediting, typesetting, and review of the resulting proof before it is published in its final citable form. Please note that during the production process errors may be discovered which could affect the content, and all legal disclaimers that apply to the journal pertain.

NIH-PA Author Manuscript
NIH-PA Author Manuscript
NIH-PA Author Manuscript

NIH-PA Author Manuscript

NIH-PA Author Manuscript

NIH-PA Author Manuscript

show that bisphosphonate-induced changes in Mohr-Coulomb material properties, including tissue shear cohesive strength, can be accurately calculated from Oliver-Pharr measurements of Young's modulus and hardness.

Keywords

Material parameter identification; Mohr-Coulomb failure criterion; Nanoindentation; Trabecular bone; Finite element method

Introduction

Nanoindentation has been widely used to study tissue mechanical properties (elastic modulus and hardness) of both cortical [1–3] and cancellous bone [4–8]. The method and equations used to calculate bone tissue modulus and hardness in these studies were based on the assumption that the bone was linearly elastic and, therefore, the material properties remained constant independent of the indentation depth [9]. In the present study, we altered the constraint of linearly elastic behavior and use nonlinear finite element analysis to determine the change in cancellous bone material properties caused by drug treatment.

Bone tissue ultrastructure and the accumulation of damage at the ultrastructural level are not completely understood [3]. In particular, the failure criterion for bone tissue at the nanoscopic level was not known until recently. Tai et al. [3] determined that a cohesive-frictional model, specifically a Mohr-Coulomb pressure dependent failure criterion (in short, Mohr-Coulomb criterion), could accurately reproduce experimental force-displacement data measured using an atomic force microscope.

In Tai et al.'s study [3], they performed a series of indentation tests on bovine cortical bone tissue using an atomic force microscope. To identify the failure properties of the tissue, they used a finite element model of the indentation process. In their models they assumed a Young's modulus of GPa and a Poisson's ratio of 0.3. They showed that the models matched the experimental data when the friction angle (ϕ) and the cohesion (c) were set to 15° and 100MPa (Fig. 1), respectively. This was an important study, because it demonstrates that the Mohr-Coulomb criterion appears to be a good material model for compressive loading of bone tissue. A limitation of the study is that their approach required assuming that the Young's modulus was fixed. In the current study, we have developed a method to determine all of the material parameters (modulus, cohesion, friction angle) except the Poisson's ratio, which we left as unchanged.

Bisphosphonates (BPs) increase average mineralization of trabecular bone tissue [10–12]. Studies in beagle dogs, using doses at and above those used for treatment of osteoporosis, have shown BP treatment also results in microdamage accumulation and a reduction in bone toughness in vertebrae [13–16]. With an increase in both bone mineralization and microdamage, it is not clear how BPs might affect bone tissue nano-level mechanical properties (elastic modulus and hardness), since mineralization and microdamage have opposite effects. The results of the current study are intended to partially clarify this mixed effect of increasing both bone tissue mineralization and microdamage because nanoindentation can directly measure the bone tissue mechanical properties.

In this study, we (1) develop a new method for identifying the material parameters of the Mohr-Coulomb criterion for bone tissue using nanoindentation; (2) determine whether the material properties identified by either of the methods (Oliver- Pharr (O-P), Continuous Stiffness Measurement (CSM), and the Mohr-Coulomb FE model) differ with bisphosphonate treatment;

NIH-PA Author Manuscript

NIH-PA Author Manuscript

NIH-PA Author Manuscript

(3) compare the material property results among the O-P, CSM and FE method, and (4) demonstrate that the material properties from the finite element results can be predicted using the Oliver-Pharr experimental results.

Materials and Methods

Bone samples

Thirty-three canine second lumbar vertebrae were used in this study. The specimens were collected during a previously completed BP treatment study [14]. Briefly, the beagle dogs were treated daily for 1 year with oral doses of alendronate sodium (ALN, 0.20 mg/kg/day, n=12), risedronate sodium (RIS, 0.10 mg/kg/day, n=10), or saline vehicle (VEH, n=11). These bisphosphonate doses approximate, on a mg/kg basis, those used for the treatment of post-menopausal osteoporosis.

The vertebrae were collected after one year of treatment and histologically processed, embedded in PMMA, and analyzed for standard bone histomorphometry [14]. The cut surface of each embedded specimen block was polished with successively finer grades of carborundum paper and polishing powders before nanoindentation.

Nanoindentation

A Nano Indenter XP system (MTS Nano Instruments, Oak Ridge, TN) was employed to measure force and displacement during indentation of the polished bone specimen. Two sites were selected randomly in two different trabeculae of each specimen using an optical microscope at 50× magnification. Using a Berkovich shape diamond indenter tip (E_i=1141GPa, ν_i=0.07), one hundred nanoindentation tests were performed at each site using a 10×10 array pattern, with 15 μm spacing in both horizontal and vertical directions. The 15 μm spacing was selected to avoid interference between different separate indentation tests, each of which left a 3 μm triangular residual cavity. The indentation procedure was under displacement control. After the surface was identified, the indenter was advanced to 500 nm at a speed of 10 nm/s to avoid the effect of bone surface roughness. A typical indentation load-displacement curve included a loading segment, a 10 second holding period at maximum load, an unloading segment, and a 50 second holding period for thermal drift measurement at 10% of maximum load (Fig. 2). Thermal drift of the nanoindentation system was calculated from the thermal drift holding segment, and used to correct modulus and hardness calculation. Due to some technical issues, such as surface approaching failure, between 60–200 nanoindentation tests finished successfully for each specimen.

A technique named Continuous Stiffness Measurement (CSM) was used to measure stiffness (S_{CSM}) during the primary loading procedure using a 2 nm magnitude oscillation with a frequency of 45 Hz. With the known frequency and the measured displacement, phase angles and force, S_{CSM} and thereafter elastic modulus and hardness can be calculated as continual functions of surface penetration depth. The unloading segment of the load-displacement curve was analyzed using a mathematical solution derived by Oliver and Pharr [8]. Two sets of elastic modulus and hardness were calculated for each specimen using the CSM method (E_{CSM} and H_{CSM}) from the loading segment [8,17] and the Oliver-Pharr method ($E_{O–P}$ and $H_{O–P}$) from the unloading segment [1,6,8,17], respectively. E_{CSM} and H_{CSM} were averaged from 200 to 500 nm in the modulus-displacement curve and the hardness-displacement curve, respectively, because the initial calculations of modulus and hardness were unstable.

Finite element model

One sixth of the nanoindentation geometry was modeled as a three-dimensional 22 finite element model in ABAQUS (ABAQUS Inc., Providence, RI) (Fig. 3). The Berkovich tip was

NIH-PA Author Manuscript

NIH-PA Author Manuscript

NIH-PA Author Manuscript

modeled as a rigid surface. A convergence study was performed to determine the required mesh size for the model. The height of modeled bone tissue was 10 μm and the radius was 16 μm. There were 300 elements in the rigid tip surface, and 5040 elements in the bone tissue block. The contact surface was assumed to be frictionless.

The isotropic form of the Mohr-Coulomb material model (Fig. 1), is controlled 6 with four parameters: (1) Young's modulus (E), (2) Poisson's ratio, (3) cohesion (c), and (4) friction angle (ϕ). The two yield parameters (c and ϕ) determine the stresses at which the material fails. Bone tissue elastic modulus (E_{FE}), and Mohr-Coulomb criterion parameters (cohesion c and friction angle ϕ) were chosen in a systematic fashion so that the results of the FE calculation (peak load and unloading stiffness) spanned the observed experimental results. No viscoelastic material property was incorporated into the finite element model, so the holding segment at the maximum load could not be simulated. In total, 1552 finite element simulations were performed (Table 1).

Material parameter identification using the Finite Element Results

By systematically varying the bone tissue elastic modulus (E_{FE}), cohesion (c) and friction angle (ϕ) of the Mohr-Coulomb material model, we were able to generate model data from the finite element results that could be matched with the experimental results. Pairs of finite element peak load and unloading stiffness were matched with experimental values from a particular nanoindentation experiment using the following *selection radius* (R):

$$R > \sqrt{\left[\left(W_F(F_{FE} - F_{Exp})\right)^2 + \left(W_S(S_{FE} - S_{Exp})\right)^2\right]}, \quad (1)$$

where F_{FE} and F_{Exp} were the maximum loads from FE simulation and experiment, respectively, and S_{FE} and S_{Exp} were the initial unloading slopes from FE simulation and experiment, respectively. From the 1552 finite element results, we were able to segregate those similar to the actual test using Eqn. 1. The parameters w_F and w_S, were used to set the relative importance of unloading slope and force in grouping the finite element results with each experimental result. In this study, w_F was selected as 1, and w_S as 100 in order that the initial unloading slope and the maximum load were represented by numbers of the same order of magnitude.

For each set of experimental nanoindentation results, a region was defined using the selection radius. If a pair of maximum load and initial unloading slope from FE simulation fell into the region, the FE simulation was considered as a matched FE simulation to the nanoindentation. The identified elastic modulus, cohesion and friction angle for each experimental nanoindentation were calculated by averaging of the material properties of the matched FE simulations (Fig. 4).

Validation of the parameter identification method

Whether the averaging method produced valid results was tested using *four randomly selected nanoindentation tests* from each group, totally tests. New FE models were built using the identified E_{FE}, c and ϕ for the nanoindentation with a selection radius of 0.25. The maximum loads of the selected nanoindentation ranged 20 from 2.36 to 6.91 mN and the initial unloading slopes were from 0.260 to 0.841 mN/nm. The maximum loads and initial unloading slopes were compared to the counterparts from experiment.

The differences in the maximum loads from FE with experiment were from −0.50% to 2.15%, and that in the initial unloading slopes were from −4.20% to 9.87%. The linear regression for the maximum loads and the initial unloading slopes from FE and experiment were:

$$F_{FE} = 1.0042 F_{Exp} (r^2 = 0.9987) \text{ and} \quad (2)$$

NIH-PA Author Manuscript

NIH-PA Author Manuscript

NIH-PA Author Manuscript

$$S_{FE}=0.9859S_{Exp}(r^2=0.9924), \quad (3)$$

where F_{FE} and F_{Exp} were the maximum loads from FE simulation and experiment of the selected specimens, respectively, S_{FE} and S_{Exp} were the initial unloading slopes from FE simulation and experiment of the selected specimens, respectively. Both the slopes of both linear regressions and r^2 values were closed to 1, which indicated the parameters identified using the averaging method were valid.

Determination of the selection radius

The selection radius was tested at 0.25 and 0.5 to determine whether it had an effect on the results. Two sets of identified E_{FE}, c and ϕ were identified and compared between the two different selection radiuses using linear regression:

$$E_{FE}\big|_{R=0.50}=0.9988 \cdot E_{FE}\big|_{R=0.25}(r^2=0.9996), \quad (4)$$

$$c\big|_{R=0.50}=1.0091 \cdot c\big|_{R=0.25}(r^2=0.9975),\text{and} \quad (5)$$

$$\phi\big|_{R=0.50}=0.9985 \cdot \phi\big|_{R=0.25}(r^2=0.5739). \quad (6)$$

The E_{FE} and c were not sensitive to the selection radius, and the errors between the differences between the identified parameters were less than 1% and r^2 values were close to 1. Identified friction angles using two different selection radiuses did not as match well (r^2=0.57), but considering the narrow range of ϕ (12.845–12.989° for R=0.50, 12.825–13.026° for R=0.25), the error was still acceptable. The following analyses were based on the identified material parameters using a selection radius of 0.25.

Statistics

The moduli and hardness measured using nanoindentation (E_{CSM}, H_{CSM}, $E_{O–P}$, and $H_{O–P}$), the identified modulus (E_{FE}), cohesion (c) and friction angle (ϕ) were first averaged over each dog specimen. The mean material parameters were compared among groups, using ANOVA and Tukey HSD as post-hoc (JMP 6, NC).

Linear regression was used to study the relationships between the measured moduli and hardness within each group. ANCOVA was used to compare differences in the relationships between the measured moduli and hardness across groups. Significant level was 0.05. Stepwise regression was used to probe the relationship between the identified material parameters (E_{FE}, c and ϕ) and the measured moduli and hardness. Linear regression was used to study significant relationships identified by stepwise regression.

Results

E_{CSM} was higher in the RIS group, but not in the ALN group, compared to the VEH group (p=0.025). No difference was observed in $E_{O–P}$ among the three groups (p=0.11, Fig. 5a). H_{CSM} and $H_{O–P}$ were significantly higher in both the ALN- and RIS- treated groups compared to VEH (p=0.002 & 0.0028, Fig. 5b), but there was no significant difference between the two BP groups.

E_{CSM} was linearly correlated with H_{CSM} in the ALN, RIS and VEH groups (r^2 =0.47, 0.74 & 0.84, p<0.018), respectively. The slopes and intercepts of the linear correlations were not different among the three groups (p=0.43 & 0.76, ANCOVA). Correlation was found between $E_{O–P}$ and $H_{O–P}$ in the RIS and VEH groups (r^2=0.59 & 4 0.75, p<0.01), but not in the ALN

NIH-PA Author Manuscript

NIH-PA Author Manuscript

NIH-PA Author Manuscript

group (r^2=0.29, p=0.071). There was no difference in the slopes and intercepts of the linear regressions between E_{O-P} and H_{O-P} in the RIS and VEH groups (p=0.41 & 0.21, ANCOVA).

The identified bone tissue moduli were 13.36±0.72 GPa in the ALN group, 13.30±1.06 GPa in the RIS group, and 12.54±0.98 GPa in the VEH group, respectively. There was no difference in E_{FE} between the three groups (p=0.085, ANOVA, Fig. 5a). The modulus estimated using finite element modeling (VEH: 12.54±0.98 GPa, ALN: 13.36±0.73 GPa, RIS: 13.30±1.06 GPa) was significantly smaller than the modulus calculated using the Oliver-Pharr (VEH: 16.78 ±1.36 GPa, ALN: 17.88±1.04 GPa, RIS:17.76±1.5 GPa) or the CSM (VEH: 19.51±1.31 GPa, ALN: 20.66±1.31 GPa, RIS:20.8±1.25 GPa) methods within each group (p<0.0001). The cohesion was significantly higher in the RIS group (131.50±1.96 MPa) than in the VEH group, and there was no difference between the ALN (126.79±1.79 MPa) and VEH (120.57±1.87 MPa) groups (p=0.001, Fig. 5c). The friction angles were around 12.91° and not different between the three groups (p=0.79, Fig. 5d).

Forward stepwise regression results showed E_{FE} was predicted by H_{CSM} and E_{O-P} (r^2=0.994, Table 2), cohesion (c) was predicted by E_{CSM}, E_{O-P} and H_{O-P} (r_2=0.988), and friction angle was only predicted by E_{O-P} (r^2=0.313). The practical ability to predict the results of the finite element method calculations using only the Oliver-Pharr results were listed in Table 3.

Discussion

At doses consistent with those used to treat post menopausal osteoporosis, both alendronate and risedronate significantly increased tissue hardness of dog vertebral cancellous bone at the nano-level. Hardness is a useful tool for estimating bone strength [18], but it is not a mechanical property in the same sense as Young's modulus, cohesion or friction angle. As a result, the goal of this study was to develop a finite element method to analyze bone tissue nanoindentation load-displacement data and determine the actual failure properties of bone tissue; cohesion and friction angle. Our method showed that the cohesion of the bone tissue was increased by bisphosphonate treatment, and this change in material properties was strongly predicted by modulus and hardness values measured using the Oliver-Pharr method. This result suggests that the increases in hardness and modulus of bone tissue calculated using the traditional Oliver-Pharr method reflect an increase in the cohesion of bone tissue after bisphosphonate treatment. The percentage increase in tissue cohesion compared to vehicle-treatment was 9% for risedronate and 5% for alendronate. These increases were not, however, statistically different from each other.

Both risedronate and alendronate resulted in higher bone tissue elastic moduli compared to control (VEH group) for the E_{CSM} measure, although no statistical difference existed between the ALN and VEH groups. For all E_{O-P}, however, an average increase with bisphosphonate treatment was observed with all being nearly significant. For E_{FE}, increases in modulus were 6.5% for alendronate and 6.1% increase for risedronate. There was no difference between the drugs in their effect of increasing modulus, by all means of estimating mechanical properties.

The modulus estimated using finite element modeling was significantly smaller than the modulus calculated using the Oliver-Pharr or the CSM method within each group. The meaning of this is unknown. However, that E_{FE} was closely predicted by E_{O-P} alone (r^2=0.989) demonstrates that both estimates are similar in their ability to discriminate changes in modulus.

The friction angle (ϕ) decreased with E_{O-P} (r^2=0.31), but no statistically significant change with bisphosphonate treatment was demonstrated. A decreased friction angle along with an increased cohesion after bisphosphonate treatment is consistent with the findings of increased overall bone strength with bisphosphonate treatment in this animal model [13,14].

NIH-PA Author Manuscript

NIH-PA Author Manuscript

NIH-PA Author Manuscript

The finite element modeling in the current study is an approach to estimate bone tissue failure properties at the nanometer level. The finite element method has been used to probe material behaviors during nanoindentation of various materials, including thin film materials [19], polymers [20] and bone [3]. In the current study, we demonstrate that the Mohr-Coulomb failure parameters of canine vertebral bone are (1) changed by treatment with bisphosphonates and (2) that the failure parameters (c and ϕ) can be predicted using the modulus and hardness estimated using the Oliver-Pharr equation. The first result is the main significance of our study, however, the broader practical importance of the study are the regressions of Table 3. With those results, the Oliver-Pharr modulus and hardness measured by nanoindentation can be associated with a modulus and a set of Mohr-Coulomb material parameters that can be used in finite element analysis.

Limitations of our study include: First, the isotropic Mohr-Coulomb failure criterion is not able to model all bone failure mechanisms. Bone tissue failure is a complex anisotropic process that cannot be fully described by such a simple criterion. Second, we ignored strain rate and time dependence of the elastic material properties. Consequently, the holding segment of the nanoindentation loading at maximum load was not simulated. Finally, we assumed a constant Poisson's ratio of 0.3 for the bone tissue. This is a commonly assumed value, but it remains an untested assumption. Bone is also known as a viscoelastic material [21,22]. The lack of viscoelastic material properties in 10 our model limits it application. The current loading and unloading speed were 10 nm/s, which is a relatively low nanoindentation test speed. For a high-speed nanoindentation, modeling bone viscoelasticity would be more important, Hence, time dependent behavior of bone tissue would play an important role in bone mechanical properties, which would be the next step for out study.

Overall, the current study introduces a new finite element method to identify the failure parameters of bone tissue based on the assumption of a Mohr-Coulomb failure surface. The finite element analysis of the experimental data demonstrates that bisphosphonate treatment increases bone hardness by increasing tissue modulus and cohesion.

Acknowledgements

This work was supported by NIH Grants AR40776 (DPF), R01 AR047838 (DBB), and T32 AR007581 (DBB), and a research grant from The Alliance for Better Bone Health (Procter and Gamble Pharmaceuticals and Sanofi-Aventis). Merck and Co. kindly provided the alendronate. This investigation utilized an animal facility constructed with support from Research Facilities Improvement Program Grant Number C06RR10601 from the NIH National Center for Research Resources. This indenter used in this study was from a support form the Office of Naval Research with a grant number of N00014-08-1-0405 (EJL).

References

1. Hoffler CE, Guo XE, Zysset PK, Goldstein SA. An application of nanoindentation technique to measure bone tissue lamellae properties. Journal of Biomechanical Engineering-Transactions of the ASME 2005;127:1046–1053.
2. Hoffler CE, Moore KE, Kozloff K, Zysset PK, Goldstein SA. Age, gender, and bone lamellae elastic moduli. Bone 2000;18:432–437.
3. Tai K, Ulm F-J, Ortiz C. Nanogranular origins of the strength of bone. Nano Letters 2006;6:2520–2525. [PubMed: 17090084]
4. Rho JY, Tsui TY, Pharr GM. Elastic properties of human cortical can trabecular lamellar bone measured by nanoindentation. Biomaterials 1997;18:1325–1330. [PubMed: 9363331]
5. Roy ME, Rho JY, Tsui TY, Evans GP, Pharr GM. Mechanical and morphological variation of the human lumbar vertebral cortical and trabecular bone. Journal of Biomedical Materials Research 1999;44:191–197. [PubMed: 10397920]

NIH-PA Author Manuscript

NIH-PA Author Manuscript

NIH-PA Author Manuscript

6. Zysset PK, Guo XE, Hoffler CE, Moore KE, Goldstein SA. Mechanical properties of human trabecular bone lamellae quantified by nanoindentation. Technology and Health Care 1998;6:429–432. [PubMed: 10100945]
7. Guo XE, Goldstein SA. Vertebral trabecular bone microscopic tissue elastic modulus and hardness do not change in ovariectomized rats. Journal of Orthopaedic Research 2000;18:333–336. [PubMed: 10815837]
8. Wang X, Rao DS, Ajdelsztajn L, Ciarelli TE, Lavernia EJ, Fyhrie DP. Human iliac crest cancellous bone elastic modulus and hardness differ with bone formation rate per bone surface but not by existence of prevalent vertebral fracture. Journal of Biomedical Materials Research Part B: Applied Biomaterials 2008;85B:68–77.
9. Oliver WC, Pharr GM. An impoved technique for determining hardness and elastic modulus using loading and displacement sensing indentation experiment. Journal of Materials Research 1992;7:1564–1583.
10. Borah B, Dufresne TE, Ritman EL, Jorgensen SM, Liu S, Chmielewski PA, Phipps RJ, Zhou X, Sibonga JD, Turner RT. Long-term risedronate treatment normalizes mineralization and continues to preserve trabecular architecture: sequential triple biopsy studies with micro-computed tomography. Bone 2006;39:345–352. [PubMed: 16571382]
11. Zoehrer R, Roschger P, Paschalis EP, Hofstaetter JG, Durchschlag E, Fratzl P, Phipps R, Klaushofer K. Effects of 3- and 5-year treatment with risedronate on bone mineralization density distribution in triple biopsies of the iliac crest in postmenopausal women. Journal of Bone and Mineral Research 2006;21:1106–1112. [PubMed: 16813531]
12. Weber M, Roschger P, Fratzl-Zelman N, Schoberl T, Rauch F, Glorieux FH, Fratzl P, Klaushofer K. Pamidronate does not adversely affect bone intrinsic material properties in children with osteogenesis imperfecta. Bone 2006;39:616–622. [PubMed: 16644299]
13. Allen MR, Burr DB. Three years of alendronate treatment results in similar levels of vertebral microdamage as after one year of treatment. Journal of Bone and Mineral Research. 2007
14. Allen MR, Iwata K, Phipps R, Burr DB. Alterations in canine vertebral bone turnover, microdamage accumulation, and biomechanical properties following 1-year treatment with clinical treatment doses of risedronate and alendronate. Bone 2006;39:872–879. [PubMed: 16765660]
15. Komatsubara S, Mori S, Mashiba T, Ito M, Li J, Kaji Y, Akiyama T, Miyamoto K, Cao Y, Kawanishi J, Norimatsu H. Long-term treatment of incadronate disodium accumulates microdamage but improves the trabecular bone microarchitecture in dog vertebra. Journal of Bone and Mineral Research 2003;18:512–520. [PubMed: 12619936]
16. Mashiba T, Turner CH, Hirano T, Forwood MR, Johnston CC, Burr DB. Effects of suppressed bone turnover by bisphosphonates on microdamage accumulation and biomechanical properties in clinically relevant skeletal sites in beagles. Bone 2001;28:524–531. [PubMed: 11344052]
17. Li X, Bhushan B. A review of nanoindentation continuous stiffness measurement technique and its applications. Materials Characterization 2002;48:11–36.
18. Wang XD, Masilamani NS, Mabrey JD, Alder ME, Agrawal CM. Changes in the fracture toughness of bone may not be reflected in its mineral density, porosity, and tensile properties. Bone 1998;23:67–72. [PubMed: 9662132]
19. Chen X, Vlassak JJ. Numerical study on the measurement of thin film mechanical properties by means of nanoindentation. Journal of Materials Research 2001;16:2974–2982.
20. Chen X, Xiang Y, Vlassak JJ. Novel technique for measuring the mechanical properties of porous materials by nanoindentation. Journal of Materials Research 2006;21:715–724.
21. Cherraf-Schweyer C, Maurice G, Taghite M, Taous K. An experimental and theoretical approach of elasticity and viscoelasticity of compact and spongy bone with periodic homogenization. Computer Methods in Biomechanics and Biomedical Engineering 2007;10:195–207. [PubMed: 17558648]
22. Lakes RS, Katz JL. Interrelationships among the viscoelastic functions for anisotropic solids: application to calcified tissues and related systems. Journal of Biomechanics 1974;7:259–270. [PubMed: 4844333]

NIH-PA Author Manuscript

NIH-PA Author Manuscript

NIH-PA Author Manuscript

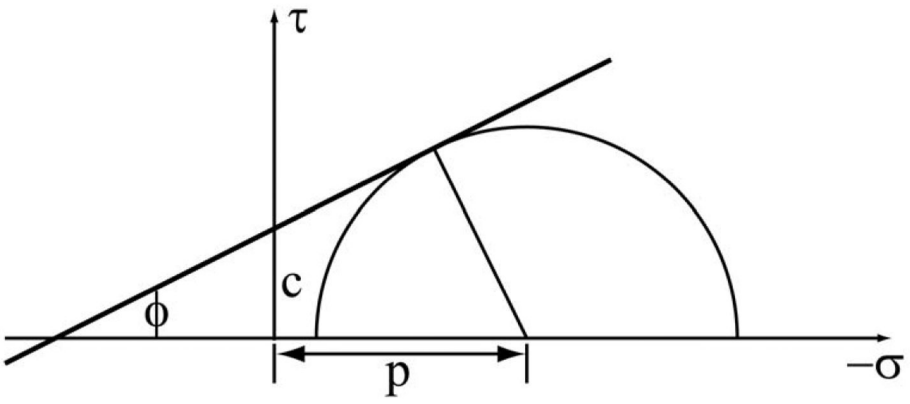

Figure 1.

In the Mohr-Coulomb material model, material failure is caused by shear stress, and the shear stress at failure is dependent upon the normal stress. . The relationship between the shear stress at failure (τ) and normal stress (σ) that defines the failure surface is $\tau=c-\sigma \tan(\phi)$, where c is the cohesion and ϕ is the friction angle. (The failure surface is a cone that is symmetric about the mean stress, therefore, this figure shows only the positive shear branch of the failure surface.)

NIH-PA Author Manuscript

NIH-PA Author Manuscript

NIH-PA Author Manuscript

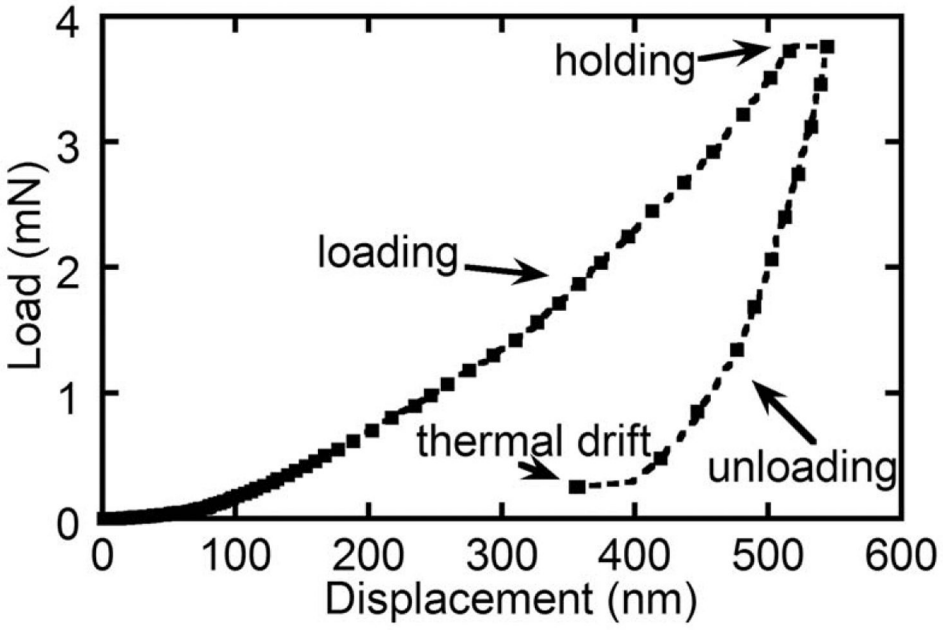

Figure 2.
A typical nanoindentation load-displacement curve, including loading, holding, unloading and thermal drift segments.

NIH-PA Author Manuscript

NIH-PA Author Manuscript

NIH-PA Author Manuscript

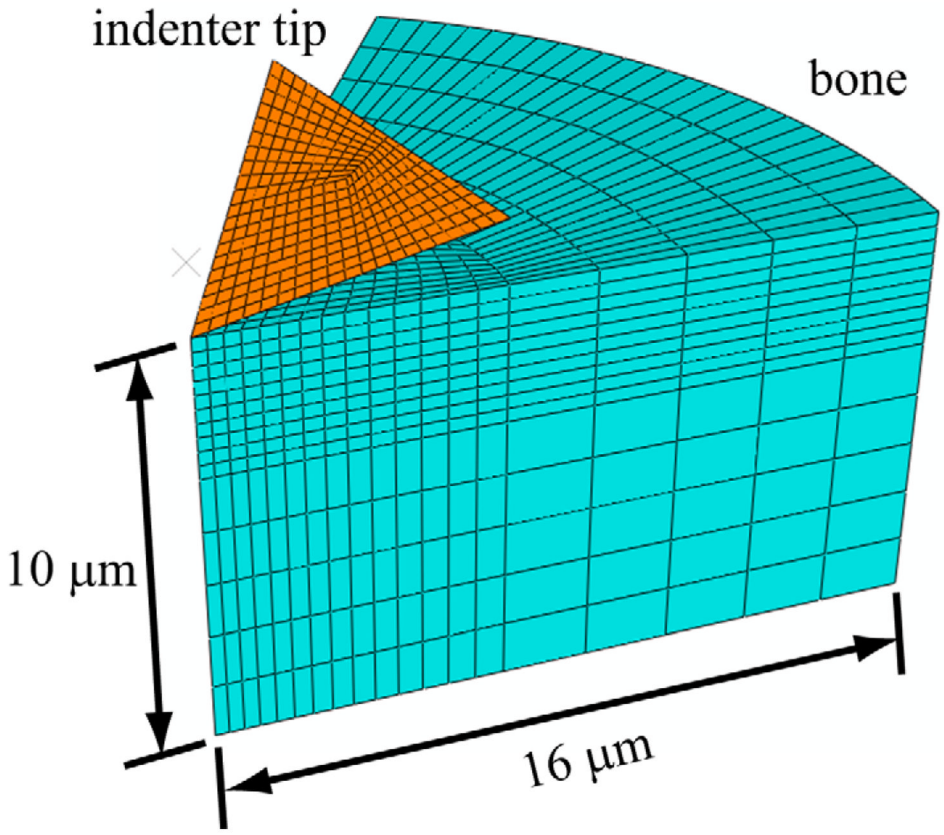

Figure 3.
One sixth of the nanoindentation was modeled as a three-dimensional finite element model in ABAQUS. The Berkovich tip was modeled as a rigid surface with 300 elements. There were 5040 elements in the bone tissue block, which had a height of 10 μm and a radius of 16 μm.

NIH-PA Author Manuscript
NIH-PA Author Manuscript
NIH-PA Author Manuscript

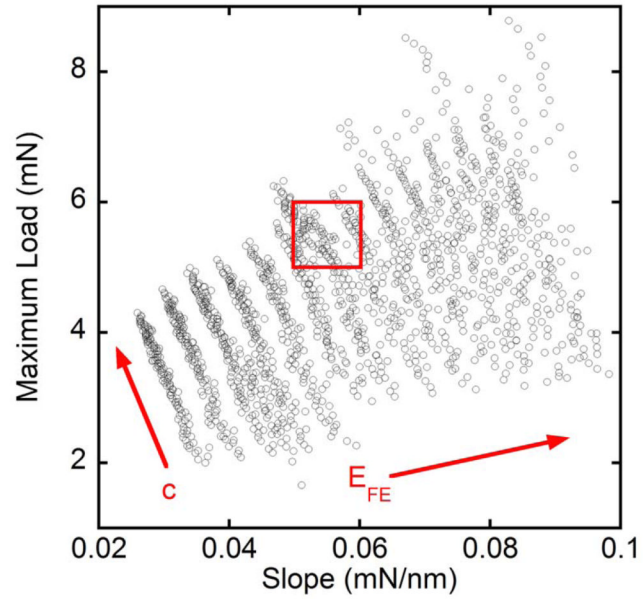

(a)

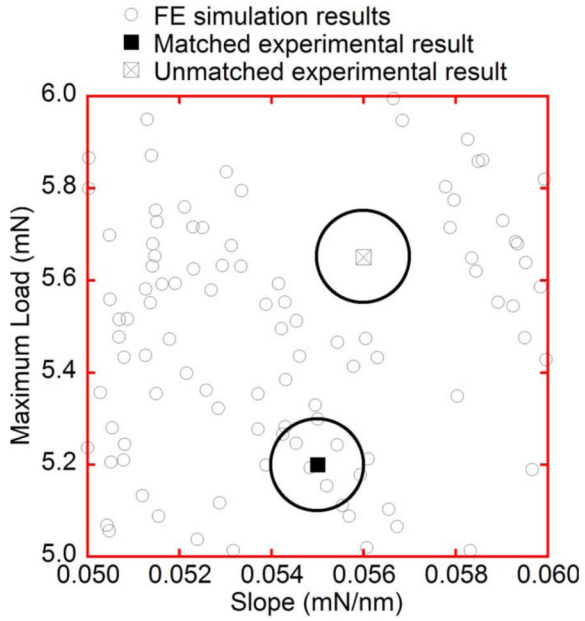

Figure 4.

(a) The maximum load vs. initial unloading slope was plotted for all FE simulations. The red arrow indicated the increasing directions of E_{FE} and c, respectively. (b) If a pair of maximum load and initial unloading slope from FE simulation fell into the defined region, the FE simulation was considered as a matched FE simulation to the nanoindentation. The identified modulus, friction angle and cohesion for each nanoindentation were calculated by averaging the input parameters of all the matched FE simulations. The black circle represented the selection region with a certain *selection radius*.

NIH-PA Author Manuscript

NIH-PA Author Manuscript

NIH-PA Author Manuscript

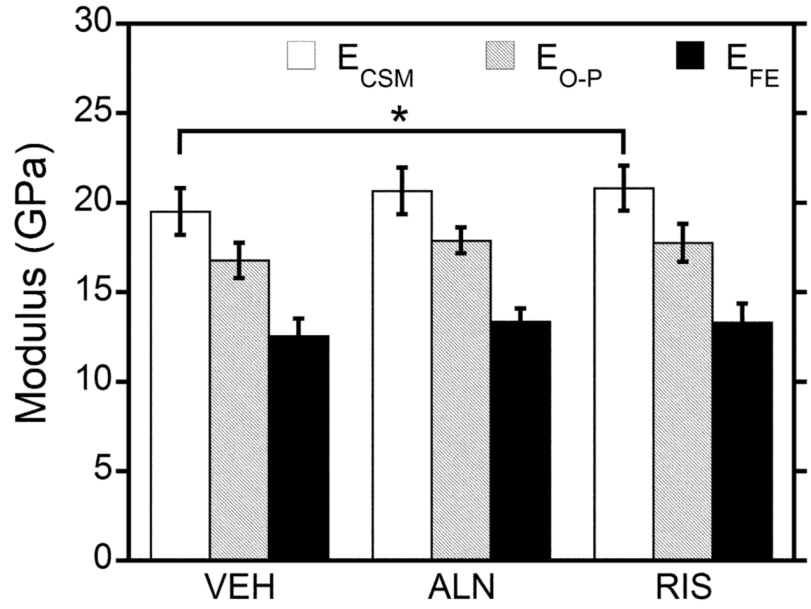

(a)

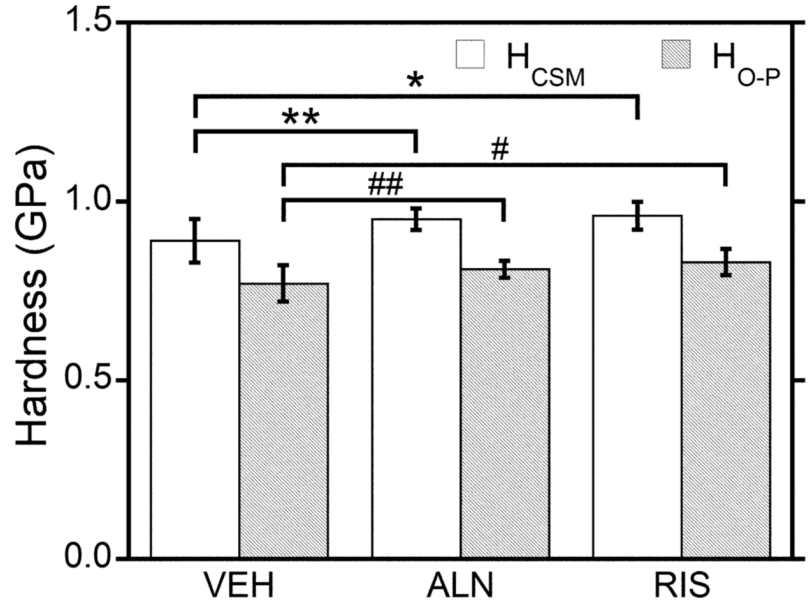

(b)

NIH-PA Author Manuscript

NIH-PA Author Manuscript

NIH-PA Author Manuscript

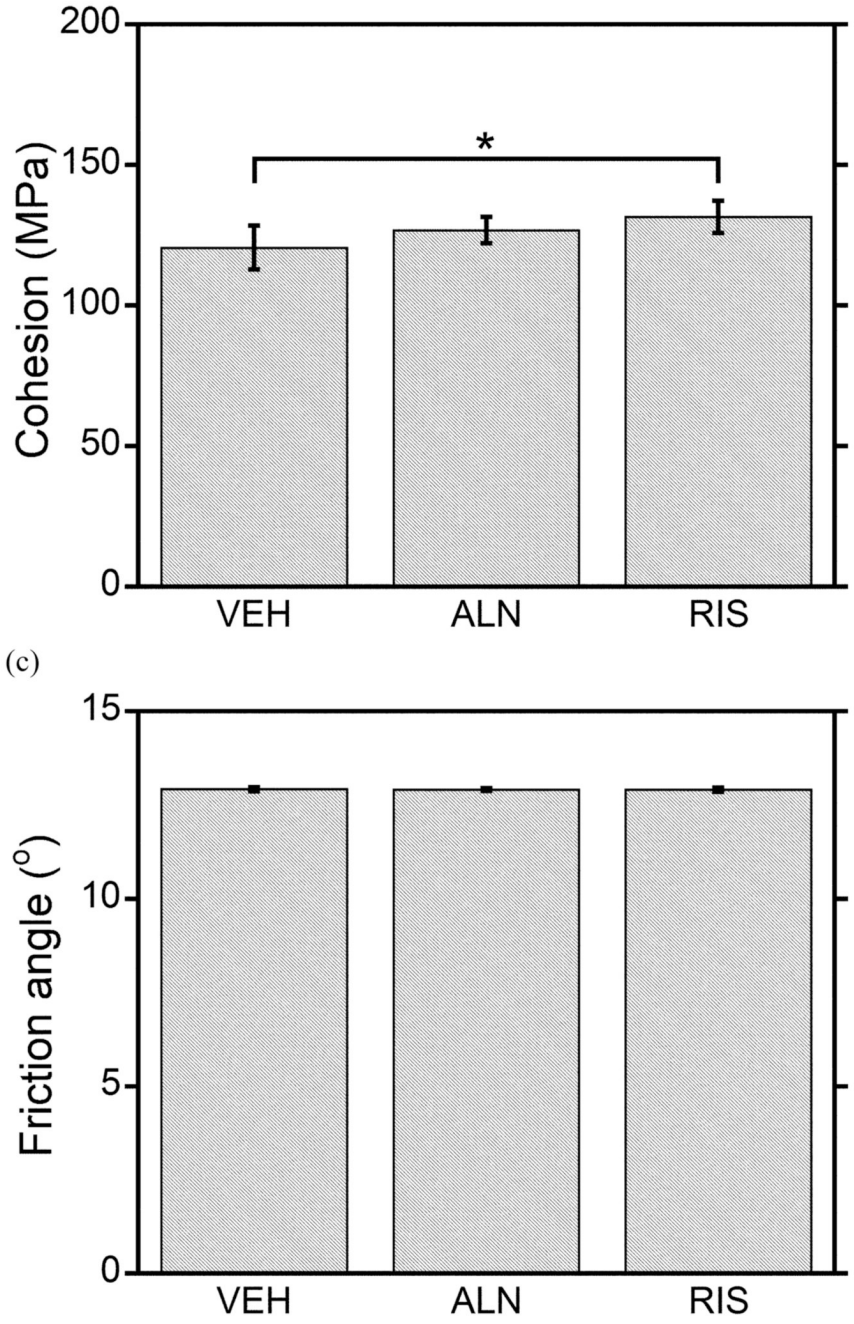

Figure 5.

(a) E_{CSM} was higher in the RIS group, but no difference in E_{O-P} or E_{FE} was found between the groups. (b) H_{CSM} and H_{O-P} in the BP treated groups were higher. (c) Cohesion (c) was higher in the RIS group than in the VEH group. (d) No difference was observed in friction angle between groups. ANOVA and Tukey- post-hoc analysis were used to compare means between the groups. Significant level is 0.05. *, **, # and # # indicate difference between groups.

NIH-PA Author Manuscript

NIH-PA Author Manuscript

NIH-PA Author Manuscript

Table 1

Lists of all FE simulation and the ranges of material parameters

Number of FE models	*E* (GPa)	$\phi^{\dagger}$(°)	$c^{\ddagger}$(MPa)
126	8	10–16	50–220
126	9	10–16	50–220
126	10	10–16	50–220
42	10.5	10–16	50–100
2	10.5	12.8*	30–40
112	11	10–16	50–200
112	12	10–16	50–200
98	13	10–16	70–200
56	13.5	10–16	180–250
98	14	10–16	70–200
98	15	10–16	70–200
98	16	10–16	70–200
10	16	12.8*	210–300
98	17	10–16	70–200
6	17	12.8*	210–260
98	18	10–16	70–200
6	18	12.8*	210–260
98	19	10–16	70–200
15	19	12.8*	210–350
98	20	10–16	70–200
6	20	12.8*	210–260
9	21	12.8*	170–250
14	22	12.8*	170–300
Total 1552	-	-	-

†The interval for ϕ is 1 °

‡The interval for c is 10 MPa

*Only one friction angle was tested

NIH-PA Author Manuscript NIH-PA Author Manuscript NIH-PA Author Manuscript

Table 2

Linear regression results between the FE indentified and experimental measured material parameters.

Dependent variable	Multiple Linear Regression Parameters						
	Independent variables					overall p-value	r^2
	E_{CSM} † (GPa)	H_{CSM} (GPa)	E_{O-P} (GPa)	H_{O-P} (GPa)	Constant (GPa)		
Elastic modulus (E_{FE}, GPa)	-‡	1.879 p<0.0001	0.6540 p<0.0001	-	−0.1088 p=0.6479	<0.0001	0.9939
Cohesion (c, MPa)	−4.509 p<0.0001	-	−5.837 p<0.0001	178.7 p<0.0001	−7.272 p=0.0189	<0.001	0.9886
Friction angle* (ϕ, °)	-	-	−0.01922 p=0.0007	-	13.25 p<0.0001	0.0007	0.3129

† Linear regression parameter and p-value were reported for each single independent variable

‡ - indicates independent parameter not used to predict dependent

* parameters have a unit of GPa^{-1}

NIH-PA Author Manuscript NIH-PA Author Manuscript NIH-PA Author Manuscript

Table 3

Linear regression results for practical prediction of FE identified parameters from Oliver-Pharr calculated modulus and hardness.

Dependent variables	Multiple Linear Regression Parameters			overall p-value	r^2
	Independent variables E_{O-P} † (GPa)	Independent variables H_{O-P} (GPa)	Constant (GPa)		
Elastic modulus (E_{FE}, GPa)	0.7118 p<0.0001	-‡	0.6301 p=0.0108	<0.0001	0.9894
Cohesion (c, MPa)	−2.732 p<0.0001	215.6 p<0.0001	0.4566 p=0.9067	<0.0001	0.9744
Friction angle * (ϕ, °)	−0.01922 p=0.0007	-	13.25 p<0.0001	<0.0007	0.3128

† Linear regression parameter and p-value were reported for each single independent variable

‡ indicates independent parameter not used to predict dependent

* parameters have a unit of °/GPa